processes

MDPI

Article

Optimization of Cr(VI) Photoreduction in Water over Ag-Promoted Nb_2O_5: Effects of Operating Conditions and Reactive Species

A. K. G. dos Santos [1], M. E. K. Fuziki [1], F. H. S. S. Pinheiro [1], M. M. Menechelli [1], A. L. W. Araujo [1], D. T. Dias [2], E. Abreu [3], Onelia A. A. dos Santos [3], T. M. Prados [4], A. M. Tusset [4] and G. G. Lenzi [1,4,*]

[1] Departamento de Engenharia Química, Universidade Tecnológica Federal do Paraná, Rua Doutor Washington Subtil Chueire, 330, Ponta Grossa 84017-220, PR, Brazil; mariafuziki@utfpr.edu.br (M.E.K.F.)
[2] Departamento Acadêmico de Física, Universidade Tecnológica Federal do Paraná, Rua Doutor Washington Subtil Chueire, 330, Ponta Grossa 84017-220, PR, Brazil
[3] Departamento de Engenharia Química, Universidade Estadual de Maringá, Avenida Colombo, 5790, Maringá 87020-900, PR, Brazil
[4] Departamento de Engenharia de Produção, Universidade Tecnológica Federal do Paraná, Rua Doutor Washington Subtil Chueire, 330, Ponta Grossa 84017-220, PR, Brazil; tusset@utfpr.edu.br (A.M.T.)
* Correspondence: gianeg@utfpr.edu.br

Abstract

Photocatalytic reduction of Cr(VI) using Nb_2O_5-based catalysts has been reported; however, Ag-promoted Nb_2O_5 remains scarcely explored. In this context, the present study describes the performance of Ag/Nb_2O_5 catalysts in removing Cr^{6+} under various experimental conditions. The catalyst was studied, maintaining the nominal metallic load of 5% Ag. To optimize the process, the following operating conditions were analyzed: pH, catalyst concentration, calcination temperature, additive, air bubbling, photolysis, and additive (hole scavenger). The results obtained indicated that the $5\%Ag/Nb_2O_5$ catalyst achieves a higher photoreduction rate than bare Nb_2O_5. Optimization of process parameters showed that the scavenger inhibits chromium adsorption on the catalytic surface. Optimal conditions observed in the tests were as follows: solution pH of 2, with hole scavenger addition, in the absence of oxygen, using a catalyst concentration of 1 g L^{-1}, and a calcination temperature of 300 °C (resulting in a poorly crystalline Nb_2O_5 phase). Photolysis in the presence of sodium formate reduced Cr^{6+}; however, the reduction was slower. In the quenching tests, the radical scavengers that most influenced the reduction of Cr^{6+} were silver nitrate (e^- scavenger) and oxalate (h^+ scavenger). Oxalate was the only one to reduce the total chromium concentration in the solution.

Keywords: hexavalent chromium removal; additive; quenching tests; Nb_2O_5

Check for updates

Academic Editor: Irene T.S. Garcia

Received: 19 August 2026
Revised: 23 September 2026
Accepted: 24 September 2026
Published: 29 September 2026

Copyright: © 2026 by the authors. Licensee MDPI, Basel, Switzerland. This article is an open access article distributed under the terms and conditions of the Creative Commons Attribution (CC BY) license.

1. Introduction

Industrialization has increased the discharge of effluents containing hexavalent chromium (Cr(VI)), posing serious environmental problems due to its toxicity and potential carcinogenicity [1]. Chromium is a naturally occurring transition metal used in industrial processes. Considered one of the most toxic heavy metals, it can exist in two predominant valence states: Cr^{3+} (trivalent chromium) and Cr^{6+} (hexavalent chromium) [2]. Trivalent chromium [Cr(III)] is considered a vital element for living beings, including humans; consequently, deficiencies or excesses of this element can significantly impact their metabolism. Cr(VI), in turn, is highly toxic and soluble, causing more severe impacts on

animals and humans [3] than Cr(III), which is insoluble and primarily bound to organic matter [4]. Effluents containing chromium can originate from various industrial processes, including tanneries, electroplating, metallurgy, steelmaking, and petrochemicals. Some processes used to remove chromium(VI) include ion exchange [5], membrane filtration [5], biosorption [3], and photocatalytic reduction [6], among others.

In particular, photocatalysis stands out for its efficiency in reducing Cr(VI) to Cr(III). The most commonly used catalysts are metal oxides and metal sulfides, including TiO_2, ZnO, WO_3, MnS, CdS, and In_2O_3. Heterogeneous photocatalysis is a simple technique for purifying water or air and can function under natural sunlight. However, several factors affect the efficiency of the photoreduction process, including the catalyst's stability, solution pH, and Cr adsorption on the catalyst, as well as the effects of additives. Another relevant factor is the band gap and the rapid recombination of photogenerated electron–hole (e^--h^+) pairs from TiO_2-based catalysts, which significantly limit their large-scale application [7]. Therefore, studies on catalyst modification to reduce the recombination of photogenerated e-h^+ pairs in these semiconductors are essential [8]. Niobium-based compounds, particularly niobium pentoxide (Nb_2O_5) and niobium-doped catalysts, have been an interesting alternative due to their high and efficient light absorption, chemical stability, and tunable electronic properties [9].

However, few studies in the literature report the use of niobium for the photoreduction of chromium, and niobium modified with Ag is scarcely described. In this context, the present work employed an Ag-promoted Nb_2O_5-based catalyst for the photocatalytic reduction of Cr^{6+} in water. Process parameters were investigated for optimization. In addition, the study investigated the impact of radical scavengers on the photoreduction of chromium.

2. Materials and Methods

2.1. Chemicals

The chemicals used in this study were: Potassium dichromate salt ($K_2Cr_2O_7$, P.A., Synth, São Paulo, Brazil); niobium pentoxide (Nb_2O_5), supplied by Companhia Brasileira de Metalurgia e Mineração (CBMM); silver nitrate P.A. A.C.S. ($AgNO_3$, Synth, Brazil), used as precursor for the Ag/Nb_2O_5 photocatalyst; absolute ethyl alcohol P.A. A.C.S. 99.5% (Synth, Brazil); sodium hydroxide (Neon, Brazil) and hydrochloric acid (Química Moderna, Brazil) for pH control.

2.2. Ag/Nb_2O_5 Catalyst Synthesis and Characterization

The Ag/Nb_2O_5 catalysts were synthesized via excess-solvent impregnation at a nominal loading of 5 wt.%. % Ag and subsequently calcined at different temperatures (300, 500, and 700 °C). This catalyst, calcined at 700 °C, was characterized by: (i) Scanning electron microscopy (SEM) and energy-dispersive X-ray spectroscopy (EDS) (Tescan Scanning Electron Microscope, Brno, Czech Republic, Vega 3 LMU equipped with dispersive energy detector—EDS-Oxford, AZTec Energy X-Act), (ii) X-ray diffraction (XRD), Shimadzu, Modelo XRD-6100, using Cu Kα radiation ($\lambda \approx 1.5406$ Å). The X-ray tube was operated at 30 kV and 30 mA. The measurements were performed in continuous-scanning mode using a θ–2θ configuration over a 2θ range of 10° to 80°. The instrumental conditions included a divergence slit of 0.5°, a scatter slit of 0.5°, and a receiving slit of 0.15 mm. Data acquisition was conducted with a scanning rate of 2° min^{-1}, a step size of 0.02°, and a counting time of 0.60 s per step. (iii) Nitrogen (N_2) physisorption measurements were carried out at 77 K using a Quantachrome Autosorb automated gas sorption system. The specific surface area was determined according to the Brunauer–Emmett–Teller (BET) method. The total pore volume was estimated at a relative pressure (P/P_0) of 0.99 using the Barrett–Joyner–Halenda

(BJH) method; (iv) Photoacoustic spectroscopy (PAS) measurements were performed in the UV–Vis region using a custom-built experimental setup. The excitation source consisted of a 1000 W xenon arc lamp (66926, Oriel Instruments, Newport Corporation, Irvine, CA, USA) coupled to a monochromator (Oriel Instruments, 74100 Cornerstone 260, Newport Corporation), while the light beam was modulated using a mechanical chopper (SR540, Stanford Research Systems, Sunnyvale, CA, USA) and the signal detected with a lock-in amplifier (SR830, Stanford Research Systems). The photoacoustic signal was acquired in a standard cell equipped with a quartz window and a capacitive microphone, and all spectra were normalized relative to a carbon black reference. The resulting spectra were employed to estimate the direct band gap energy using linear approaches.

2.3. Photocatalytic Tests

Photocatalytic tests were performed in a batch system. These tests consisted of 30 min of adsorption in the dark, followed by 120 min of photocatalysis under UV irradiation. The system consisted of a 250 mL borosilicate reactor with a cooling jacket, a 220 W mercury-vapor lamp (without the protective lamp), a magnetic stirrer, an atmospheric air pump, and a thermostatic bath to maintain a temperature of 293 K. In the tests, pH adjustment was performed using HCl and NaOH solutions. The studied pH values were 2.0, 4.8 (the natural solution's pH), and 7.0. Catalyst concentration was varied from 0.5 to 1.0 $g \cdot L^{-1}$, and the tests were performed with and without O_2 bubbling. Quenching tests were performed to identify the main active species in Cr^{6+} photoreduction. Isopropanol (2 mM), benzoquinone (2 mM), oxalate (2 mM), and Silver Nitrate (2 mM) were used as $^{\bullet}OH$, $O_2^{\bullet -}$, h^+, and e^- scavengers, respectively. The following flowchart describes the test sequence (Figure 1).

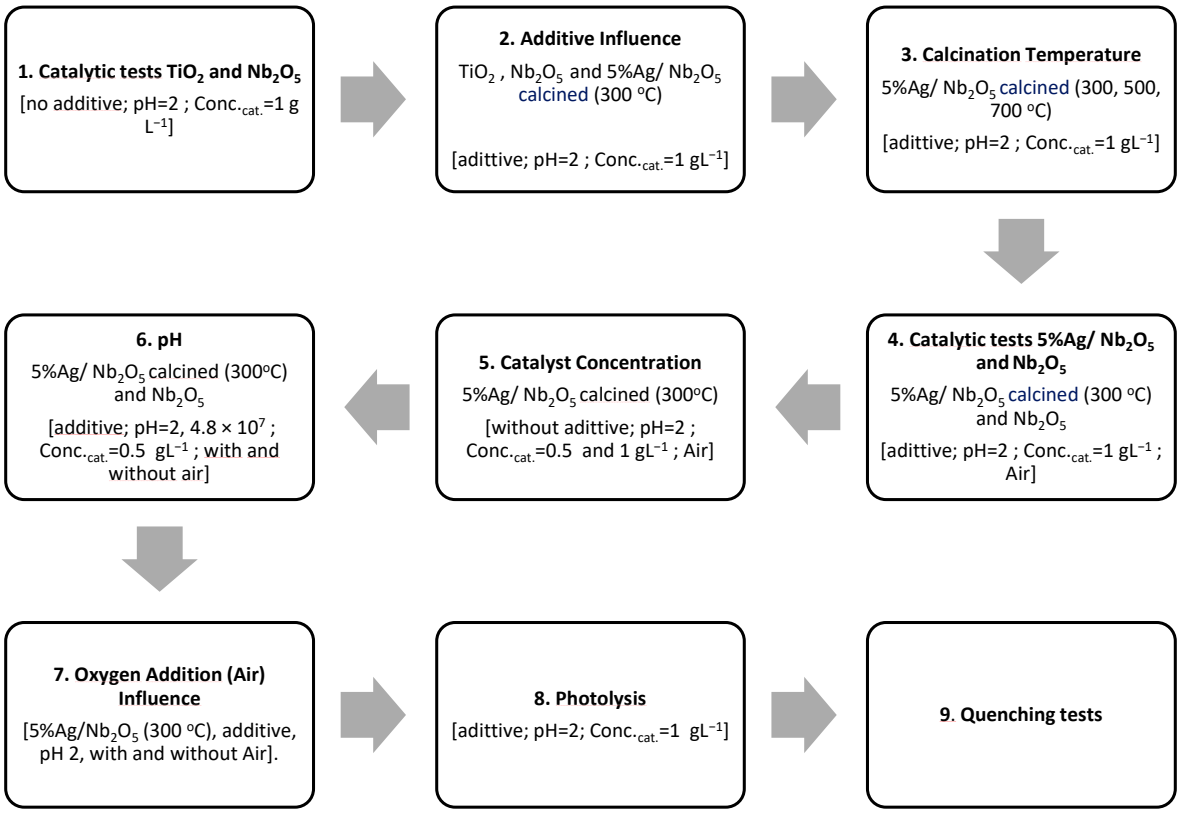


Figure 1. Flowchart detailing the sequence of experimental tests.

3. Results and Discussion

3.1. Nb_2O_5 and TiO_2 Catalysts

Figure 2 presents a comparison of the performance of Nb_2O_5 and TiO_2 catalysts in removing Cr^{6+} under the same conditions. The results indicated that Nb_2O_5 was more efficient in removing Cr^{6+} (~70%), with approximately 54% removal occurring in the first 30 min of adsorption in the dark. Even disregarding the contribution of adsorption, niobium pentoxide showed a slightly greater photocatalytic reduction of Cr^{6+}, confirming its suitability for application in the reduction of hexavalent chromium.

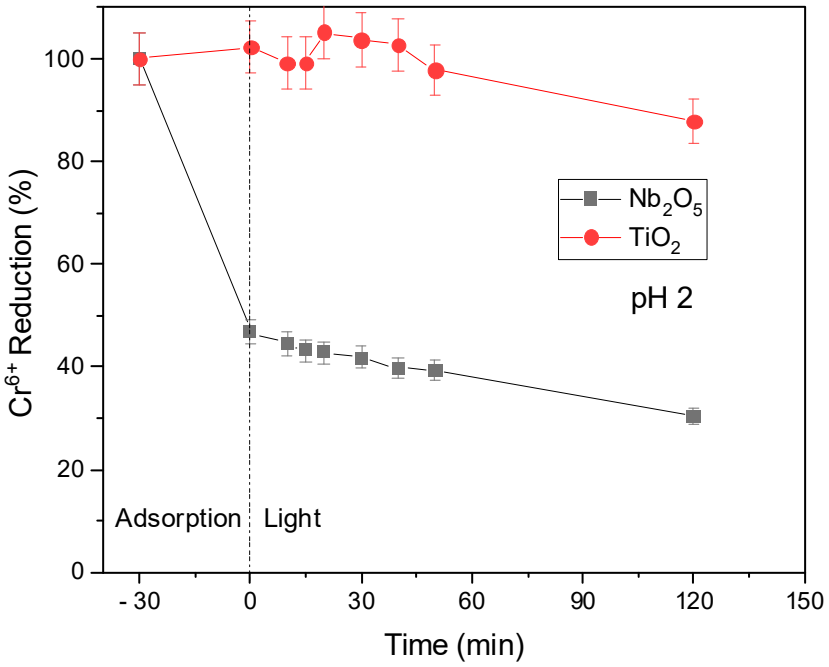


Figure 2. Adsorption and photocatalysis results using non-calcined TiO_2 and Nb_2O_5 catalysts [1 g L^{-1}, without additive, pH 2].

Furthermore, as shown in Table 1, the surface area of Nb_2O_5 is significantly larger than that of TiO_2, which explains the more efficient adsorption process. Other relevant characteristics include the smaller band gap of Nb_2O_5 (3.09 eV) compared to TiO_2 (3.61 eV), which means the energy required to go from the valence band to the conduction band is lower, favoring the process. In the literature, a band gap of 3.2 eV is reported for TiO_2 [10]; however, in this work, commercial TiO_2 was used without heat treatment. The point of zero charge for TiO_2 and Nb_2O_5 was 6.0 and 6.6, respectively.

Table 1. Specific area, pore volume, band gap, and PCZ of the catalysts.

Catalyst	Specific Area (m^2 g^{-1})	Pore Volume (cm^3 g^{-1})	Band Gap (eV)	PCZ
TiO_2	17	0.0223	3.61	6.0
Nb_2O_5	182	0.1727	3.09	6.6

3.2. Influence of the Additive

A commonly used strategy in heavy-metal photocatalytic reduction is to add an additive or organic sacrificial agent to the reaction system to capture the photogenerated holes and enhance the photocatalyst's effectiveness. The tests evaluating the influence of the additive on the photocatalytic reaction are presented in Figure 3. These results show that the addition of sodium formate, a hole scavenger, to the solution led to a greater

reduction of Cr^{6+} in the photocatalytic process, thereby favoring the photocatalytic kinetics, with approximately 97% chromium reduction. On the other hand, a marked decrease in chromium adsorption on the material's surface was observed.

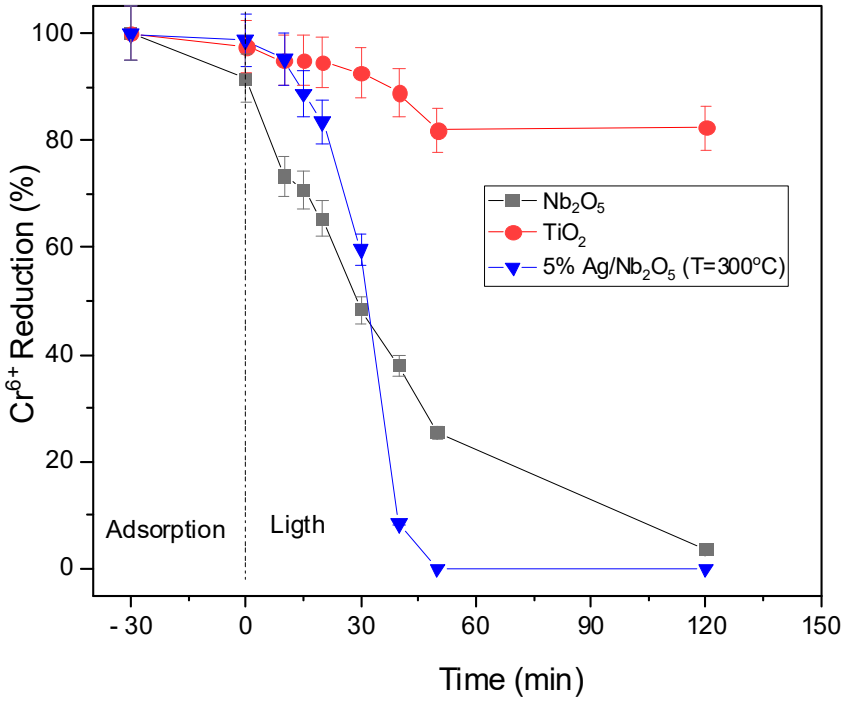


Figure 3. Photocatalytic results obtained using the TiO_2 and Nb_2O_5 (non-calcined) and 5%Ag/Nb_2O_5 (calcined at 300 °C) [1 g L^{-1}, additive, pH 2].

Similar results have also been reported in the literature for other reactions [11]. Guo et al. (2016) examined the photocatalytic reduction activity of U(VI) in ZnO/hectorite. They found that as the amount of additional methanol increased, the rate of U(VI) reduction increased significantly, whereas no U(VI) reduction occurred in the absence of methanol [12]. Similarly, Le et al. (2020) investigated the photocatalytic reduction of U(VI) using gC_3N_4. The results revealed that the reaction could not proceed without the addition of methanol as an additive (sacrificial agent), and that the reduction efficiency increased to approximately 90% upon its addition [13]. In their study on the reduction of Cd ions using TiO_2, Nguyen et al. [11] highlighted that the addition of formate ions was crucial for the reduction of the metal, and that both the addition of the metal ion and the hole scavenger were fundamental for the process. The authors observed that the addition of formate ions to the solution favored the adsorption of chromium, since the organic ions also acted as an anchor, facilitating the adsorption of Cd, in addition to altering the zeta potential of the catalyst surface to more negative values, favoring the electrostatic interactions of the surface with the positive Cd ions [11]. In the present case, however, the chromium ions are predominantly in the negatively charged form, so the addition of formate ions hinders their adsorption onto the Nb_2O_5 surface.

Comparing the performance of the catalysts in the presence of sodium formate (Figure 3), it is observed that the 5%Ag/Nb_2O_5 catalyst calcined at 300 °C showed the highest percentage of Cr(VI) removal. The result suggests that Ag added to the catalyst increased the Cr(VI) removal efficiency. Similarly, the incorporation of transition metals into photocatalysts has been reported to facilitate charge-transfer processes, associated with the role of transition metals as electron reservoirs [14]. Ag incorporated into photocatalysts has been reported to favor the storage of photogenerated electrons and facilitate their transfer

to Cr(VI), promoting its reduction [15]. Considering this, the 5%Ag/Nb_2O_5 catalyst was selected for the following photocatalytic tests.

3.3. Influence of Calcination Temperature (5%Ag/Nb_2O_5)

The results of the influence of calcination temperature (300, 500, and 700 °C) on the 5%Ag/Nb_2O_5 catalyst are presented in Figure 4. It was possible to achieve complete removal of hexavalent chromium regardless of the calcination temperature of the photocatalyst. However, the reduction rate was higher for the catalyst calcined at 300 °C. Furthermore, the adsorption process was insignificant under the conditions studied. The 5%Ag/Nb_2O_5 catalyst calcined at 300 °C exhibited faster reduction kinetics, i.e., a higher reaction rate constant. Lenzi et al. [16] indicated that the 5%Ag/Nb_2O_5 catalyst calcined at 700 °C showed the presence of $AgNb_7O_{18}$ and $AgNb_{13}O_{33}$ in the sample. These phases can only be obtained from Ag and Nb_2O_5 precursors calcined at high temperatures. Considering pure niobium pentoxide, Fidelis et al. [9] observed that non-calcined Nb_2O_5 samples, initially with an amorphous structure, transformed into TT and T-Nb_2O_5 crystalline phases when calcined at temperatures above 673 K (773–873 K).

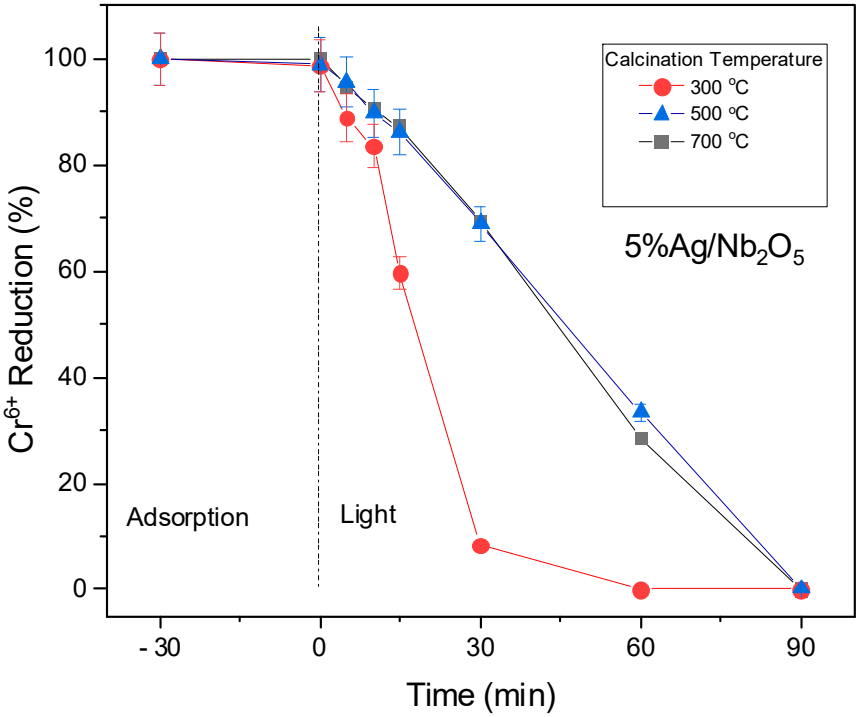


Figure 4. Photocatalytic results using calcined 5%Ag/Nb_2O_5 catalysts [1 g L^{-1}, additive, pH 2, without air].

3.4. Catalyst Characterization

X-ray diffraction (XRD): The results of the diffractograms of the 5%Ag/Nb_2O_5 catalyst calcined at temperatures of 300, 500, and 700 °C are shown in Figure 5. Based on the diffractogram analysis (Figure 5), the increase in catalyst crystallinity with increasing calcination temperature is evident. Furthermore, it was observed that calcination at 700 °C promoted the conversion of the crystalline phase, leading to the formation of silver and niobium oxides ($AgNb_{13}O_{33}$ and $AgNb_7O_{18}$), as previously reported by Lenzi et al. [16], in contrast to the predominance of niobium pentoxide in the samples calcined at 300 °C and 500 °C. In the literature, $AgNb_7O_{18}$ and $AgNb_{13}O_{33}$ phases have been described as perovskite-like structures and were obtained following heat treatment at 600 °C for 3 h, followed by treatment at 800 °C for 3 h [17,18]. These phases were also reported by Rozier

and Szajwaj [19] as part of the Ag_2O–Nb_2O_5 system, in which phase formation and stability are strongly influenced by composition and temperature. In this context, heat treatment can directly affect crystal structure through processes such as recrystallization, microstructural homogenization, phase redistribution, and grain growth, as reported by Liu et al. for Ag-based alloys [20]. Although it was not possible to identify peaks related to silver, evidence of its presence in the catalysts was detected in the photoacoustic spectroscopy analyses.

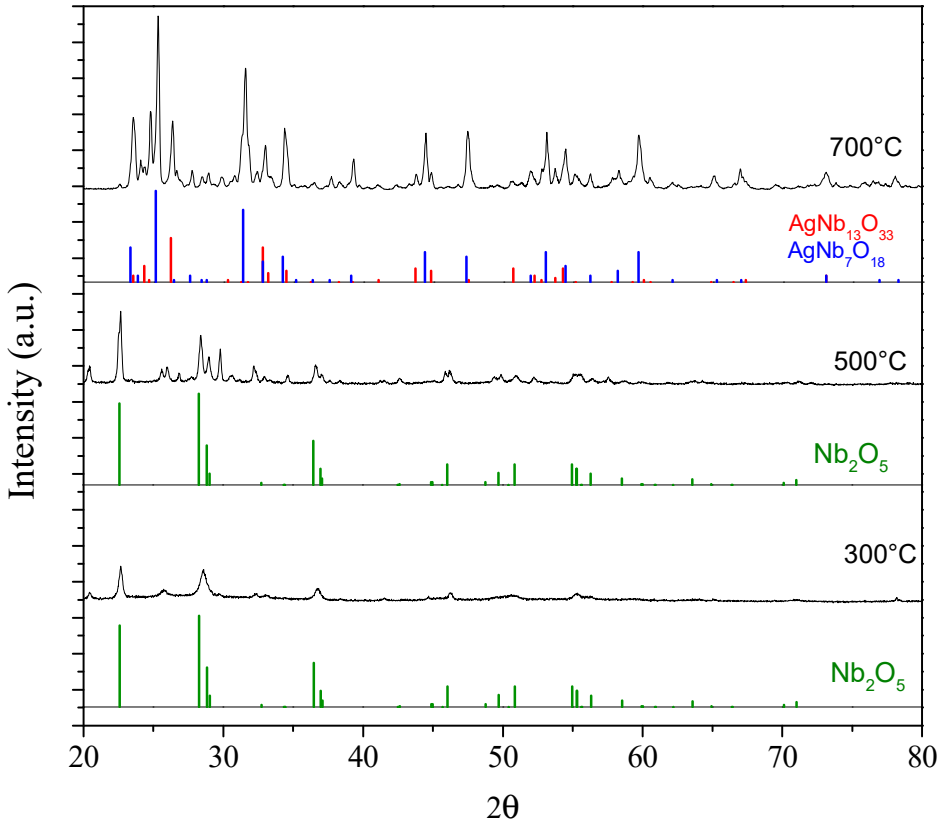


Figure 5. Diffractogram of 5%Ag/Nb_2O_5 catalysts calcined at 300, 500 and 700 °C.

Photoacoustic spectroscopy (PAS): The UV-Vis absorption spectra of 5%Ag/Nb_2O_5 catalysts calcined at 300, 500, and 700 °C are shown in Figure 6. They presented broad bands at 225–425 nm and 425–600 nm. Nb_2O_5 oxide shows overlapping absorption bands in the first region mentioned, and silver in the second region. Given the phase difference ($\Delta\psi$), there are two distinct absorption centers within overlapping absorption bands. Due to experimental error, $\Delta\psi$ must be greater than 1°. After phase-spectral separation (PRPA), the overlapping absorption bands were separated, and Table 2 presents the absorption centers and their assignments.

It is observed that the oxides exhibited a redshift with increasing calcination temperature, both for the absorption bands corresponding to niobium nanodomains and for the plasmon resonance (SPR) bands characteristic of Ag nanoparticles.

Possibly, increasing the calcination temperature increased nanoparticle size, as the absorption peak shifted to longer wavelengths (redshift). This directly affects catalytic activity: the smaller the particle size, the greater the surface area and the availability of active sites, thereby favoring the process.

According to Table 2, PRPA also showed more than one absorption peak for silver ($\Delta\psi_{i\text{-}j} > 1°$), indicating a possible anisotropic, non-spherical particle shape. It was also observed that the phase difference ($\Delta\psi_{i\text{-}j}$) between the absorbing centers for silver doubled

with the increase in calcination temperature to 700 °C. On the other hand, the phase difference between the absorption peaks of Nb_2O_5 remained at 2°.

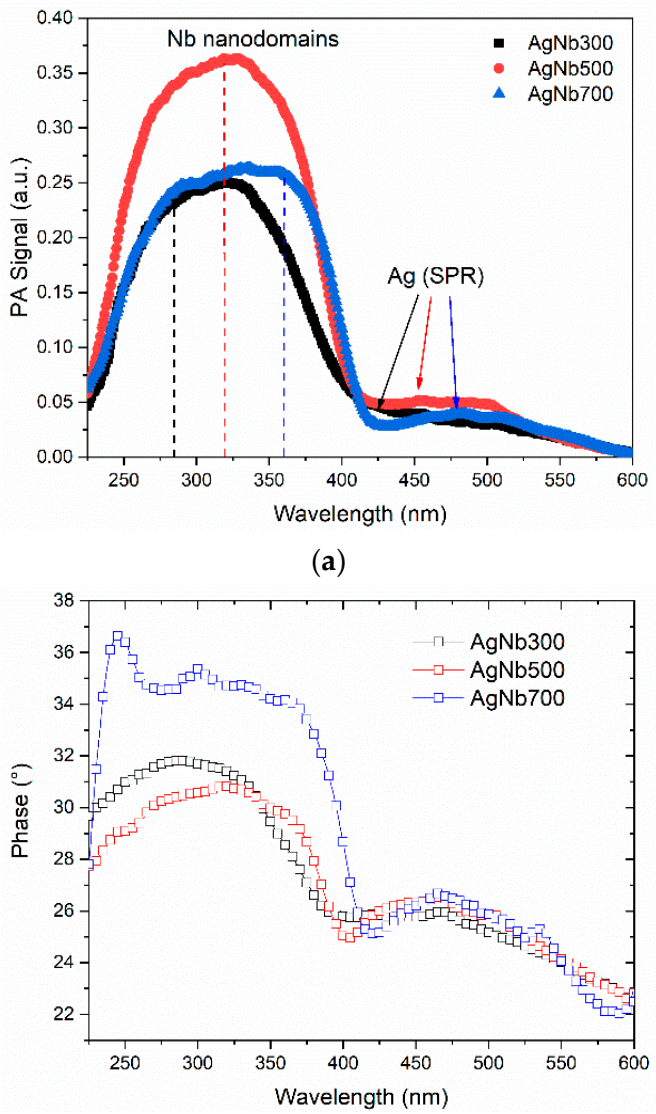


Figure 6. Photoacoustic (P.A.) spectra of 5%Ag/Nb_2O_5 samples calcined at different temperatures (300, 500, and 700 °C), showing (**a**) P.A. signal intensity and (**b**) corresponding phase spectra as a function of wavelength.

Figure 7 below shows only the SPR band after applying the PRPA method (zeroing out the Ag peak around 550 and 575 nm). The reduction of silver ions (Ag^+) to metallic silver (Ag^0) can be confirmed by the appearance and increase in the intensity of the absorption peak (SPR), and by an increase in the intensity of the P.A. signal with increasing calcination temperature. This result indicates that at 300 °C, the reduction began and silver nanoparticles (AgNPs) formed, and that as the calcination temperature increased, the concentration of AgNPs increased (as evidenced by the increased absorption intensity of the characteristic SPR band).

Table 2. Results from the absorption and allocation centers.

Sample	Center nm	Referent to	$\Delta\psi_{i-j}$ (°)
Ag/Nb_2O_5 300 °C	226	* LMCT from O^{2-} to Nb^{5+}	2
	285	Nb nanodomains (probably NbO_6 octahedra sharing vertices)	
	425	Ag—surface plasmon resonance (SPR)	2
	550	Ag	
Ag/Nb_2O_5 500 °C	240	* LMCT from O^{2-} to Nb^{5+}	2
	318	Nb nanodomains	
	450	Ag-SPR	2
	550	Ag	
Ag/Nb_2O_5 700 °C	246	* LMCT from O^{2-} to Nb^{5+}	2
	360	Nb nanodomains	
	475	Ag-SPR	4
	575	Ag	

* ligand–metal charge transfer (LMCT).

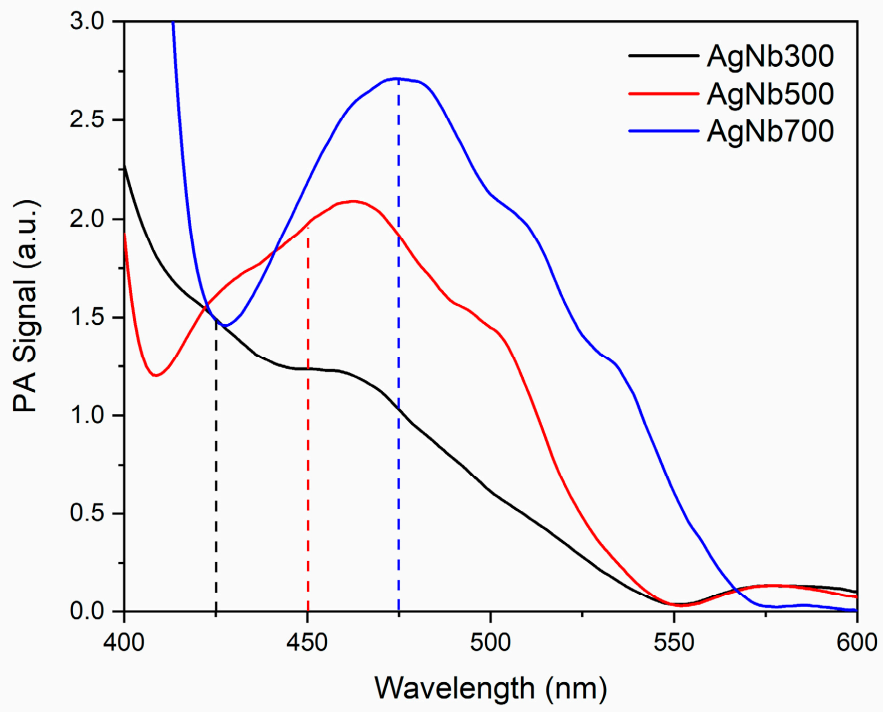


Figure 7. SPR band after PRPA method.

The band gap results (Table 3) were obtained using the Linear Method, Equation (1),

$$(a(h\nu))^2 = A(h\nu - E_g) \quad (1)$$

Based on previous results, the band gap for Nb_2O_5 was estimated at approximately 3.15 and 3.20 eV (400 °C) and 3.04 and 3.05 eV (800 °C) using PAS [21] and UV diffuse reflectance [22], respectively. PAS also previously estimated the energy band for silver at 3.37 eV [23], whereas the literature reports 3.4 eV for silver nanoparticles [24] and values between 1.84 and 2.20 eV for thin films [25].

Table 3. Band gap results.

Catalyst	Eg 1 (eV)	Eg 2 (eV)	Eg 3 (eV)	Previous References
AgNb300	3.02	2.41	-	
AgNb500	3.01	2.22	-	
AgNb700	2.98	2.30	2.18	
Nb_2O_5 400 °C	3.15/3.20	-	-	[21,22]
Nb_2O_5 800 °C	3.04/3.05			[21,22]
Ag	3.37	-	-	[23]

The estimated band gap energy for 5%Ag/Nb_2O_5 300 °C and 5%Ag/Nb_2O_5 500 °C resulted in two distinct optical band energies, Eg1 and Eg2, which corresponded to 3.02 and 2.41 eV for 5%Ag/Nb_2O_5 300 °C and 3.01 and 2.22 eV for 5%Ag/Nb_2O_5 500 °C (Figure 8).

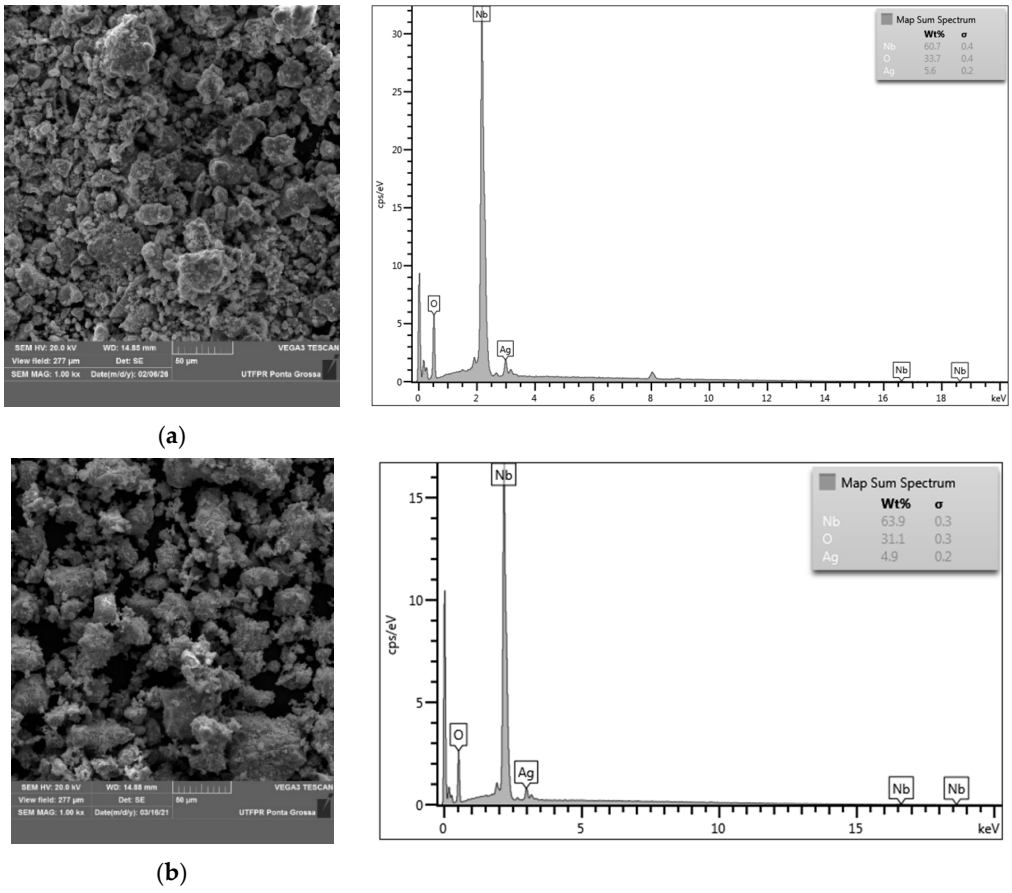


Figure 8. SEM/EDS results for the 5%Ag/Nb_2O_5 samples calcined at (**a**) 300 °C; (**b**) 700 °C.

The first gap is probably due to Nb_2O_5, and the second to silver. The sample calcined at 700 °C also showed an intermediate gap, with a third gap of lower value than those of the previous samples, consistent with previous discussions of the photoacoustic signal and phase.

Scanning Electron Microscopy–Energy Dispersive X-ray Spectroscopy (SEM–EDS): The results of the micrographs are shown in Figure 8.

PAS analysis indicated that at 300 °C, a rougher surface with smaller particles was present. Furthermore, at the analyzed point, there was greater Ag exposure on the catalytic surface compared to the portion analyzed for the catalyst calcined at 700 °C.

3.5. Influence of pH, Catalyst Concentration, Oxygen Addition, and Photolysis

Tests were conducted to assess the effects of pH, catalyst concentration, and oxygen (air) on the photocatalytic reduction of chromium(VI). Although the 5%Ag/Nb_2O_5 catalyst showed similar performance across different calcination temperatures, the material calcined at 300 °C was selected for its higher reaction rate compared with the other 5%Ag/Nb_2O_5 catalysts and the non-calcined Nb_2O_5. Additive (sodium formate) and oxygen (air) were also employed. Figure 9a presents the results of the experiments comparing 5%Ag/Nb_2O_5 calcined at 300 °C and the non-calcined Nb_2O_5, while Figure 9b illustrates the effect of catalyst concentration on Cr(VI) reduction.

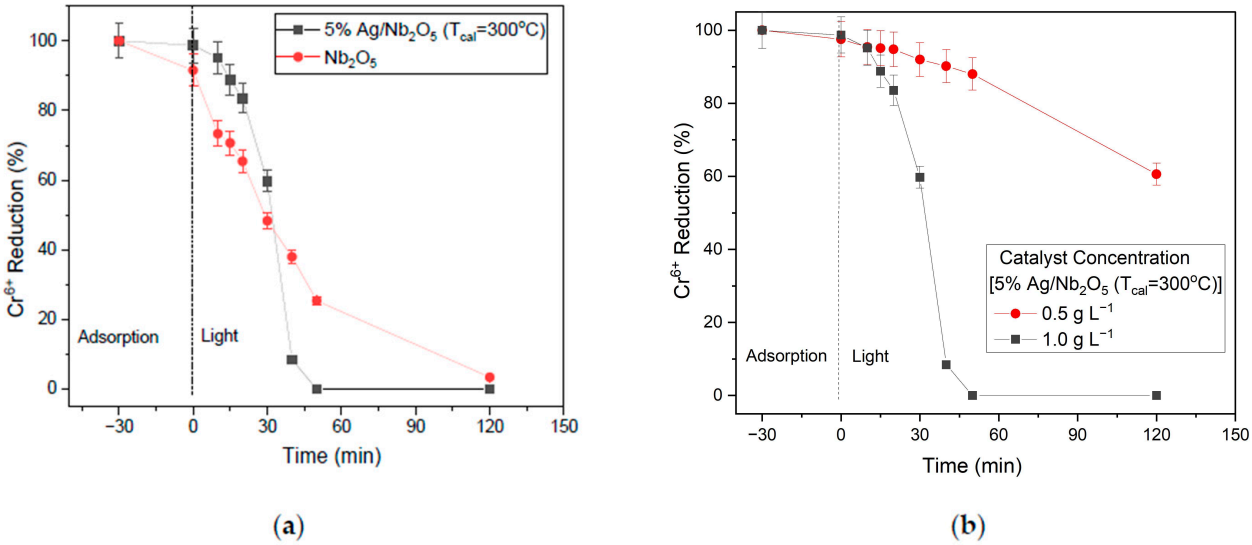


Figure 9. Photocatalytic results using the catalysts: (**a**) 5%Ag/Nb_2O_5 (300 °C) and Nb_2O_5, [1 g L^{-1}, additive, pH 2, without air]. (**b**) Influence of catalyst concentration 0.5 and 1 g L^{-1} [5%Ag/Nb_2O_5 (300 °C), additive, pH 2, without air].

The effect of pH was evaluated under acidic and neutral conditions. The results obtained are shown in Figure 10a (5%Ag/Nb_2O_5 calcined at 300 °C) and Figure 10b (Nb_2O_5).

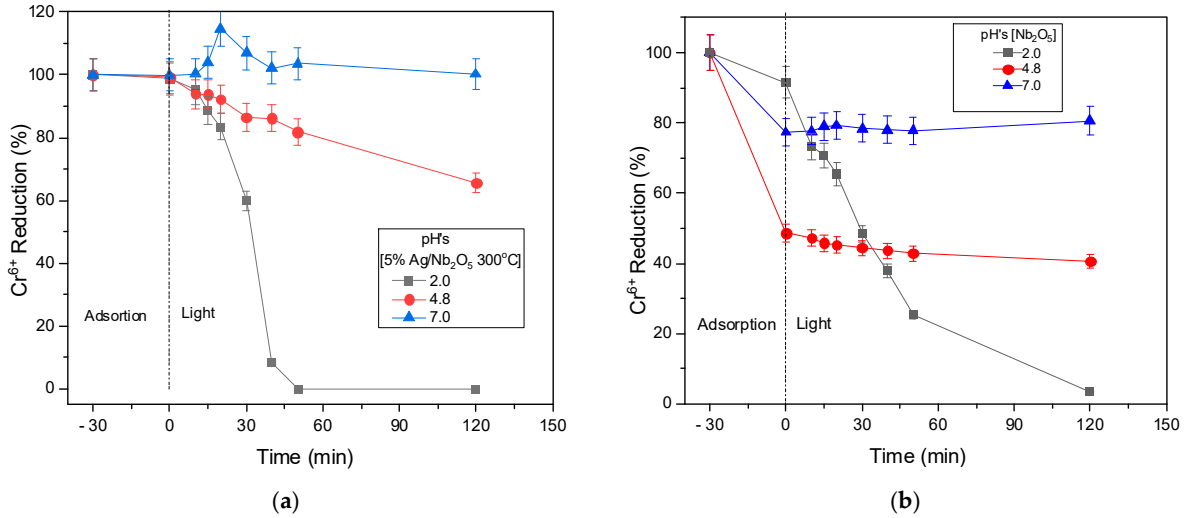


Figure 10. Photocatalytic results at different pHs: (**a**) [5%Ag/Nb_2O_5 (300 °C), additive, 1 gL^{-1}, without air] (**b**) [Nb_2O_5, additive, 1 gL^{-1}, without air].

In the photocatalytic tests, the optimal pH for both catalysts was 2. This result is consistent with the description by Josué et al. [6], who reported that highly acidic condi-

tions enhance the performance of this type of catalyst by improving adsorption on the catalyst surface.

Figure 11 shows the results of the photocatalytic process, confirming the effect of adding oxygen supplied by an air pump.

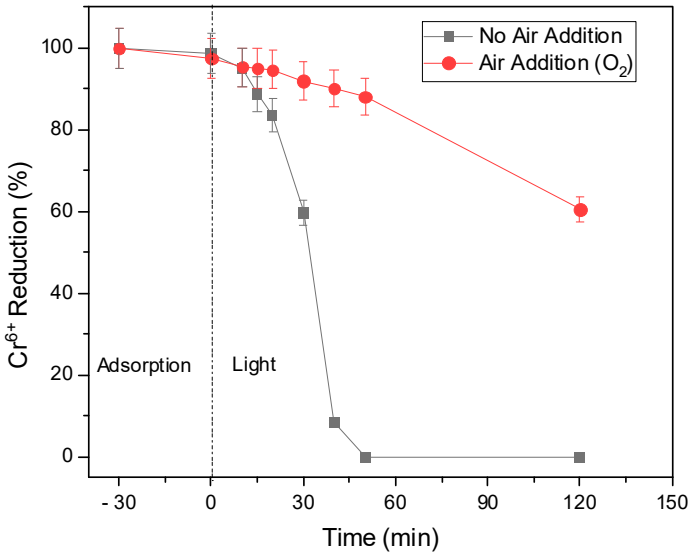


Figure 11. Photocatalytic results with and without the presence of Air [5%Ag/Nb_2O_5 (300 °C), additive, pH 2].

A photolysis test to verify the reduction of chromium(VI) using only radiation (photolysis) was performed, as shown in Figure 12. To complement the effect of photolysis on the process, tests were also carried out with 0.001 and 0.01 M concentrations of SF but without the addition of a photocatalyst. Although a significant reduction occurs, the process is slower, which would not be suitable for a continuous process, for example. Sodium formate plays an important role in the reduction of chromium and in the formation of radicals from photolysis and/or photocatalysis, as observed by Cappelletti et al. [26].

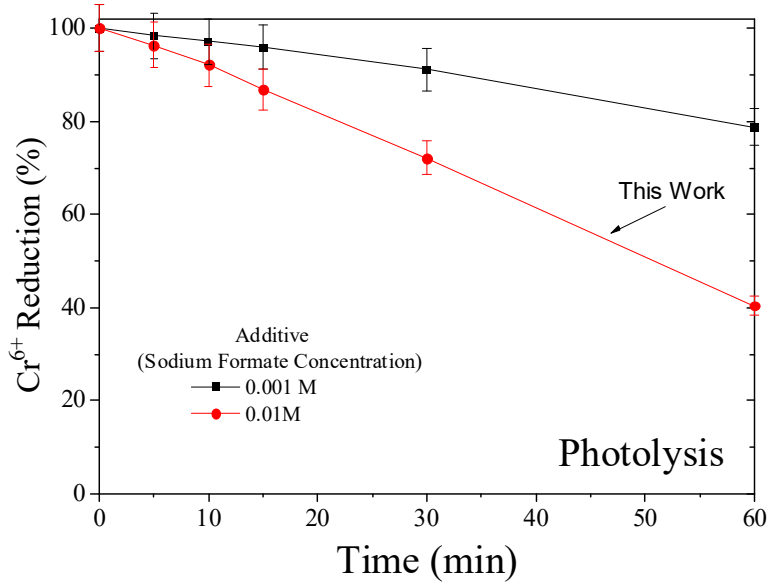


Figure 12. Photolysis Results [Additive (0.01 and 0.001 M Sodium Formate), pH 2, without air].

3.6. Quenching Tests—Contribution of Radicals

Photocatalytic tests (Figures 13 and 14) were carried out in the presence of radical scavengers (oxalate, silver nitrate, benzoquinone, and isopropanol) to assess the effects of h^+, e^-, $O_2^{\bullet -}$ and $^{\bullet}OH$ on the reaction mechanism. Oxalate, a hole (h^+) scavenger, significantly affected Cr(VI) reduction: in its presence, Cr(VI) removal reached approximately 13% after 50 min and 56% after 120 min, whereas total chromium (Cr^{+6} and Cr^{+3}) removal was only 11%. In the presence of benzoquinone, a superoxide radical ($O_2^{\bullet -}$) scavenger, Cr(VI) reduction achieved 76% in 50 min and 87% in 120 min. Using silver nitrate, an electron (e^-) scavenger, Cr(VI) reduction reached about 23% after 50 min and 50% after 120 min. When isopropanol, a hydroxyl radical ($^{\bullet}OH$) scavenger, was added, Cr(VI) reduction was approximately 33% at 50 min and 77% at 120 min. It is important to note that under standard conditions (without scavengers), Cr(VI) reduction reached 100% after 50 min. These results suggest that photogenerated electrons and holes are the main contributors to Cr(VI) reduction, as evidenced by the more pronounced inhibition observed in the presence of $AgNO_3$ and ammonium oxalate. The smaller effects observed with benzoquinone and isopropanol suggest that $^{\bullet}O_2^-$ and $^{\bullet}OH$ may have secondary roles in the overall process.

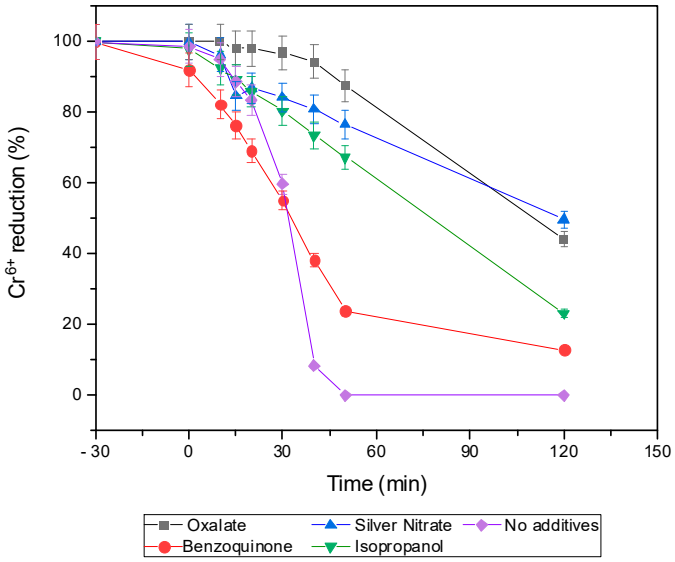


Figure 13. Photocatalytic kinetic results for Cr(VI) reduction in the presence of scavengers [5%Ag/Nb_2O_5 (300 °C), additive, pH 2, 1 gL^{-1}, without Air].

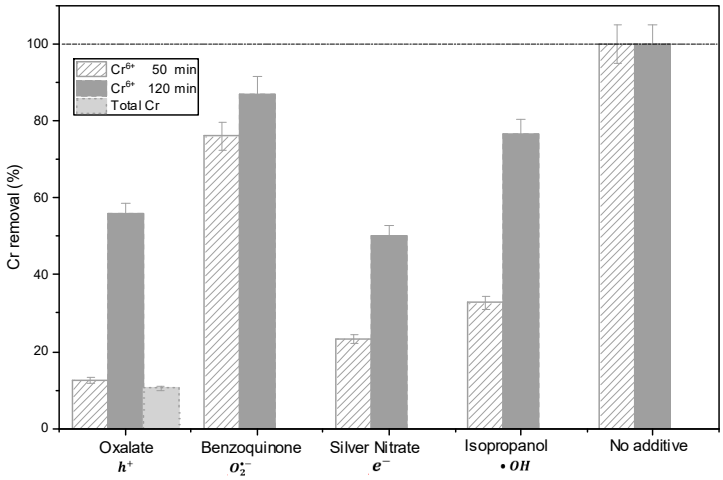
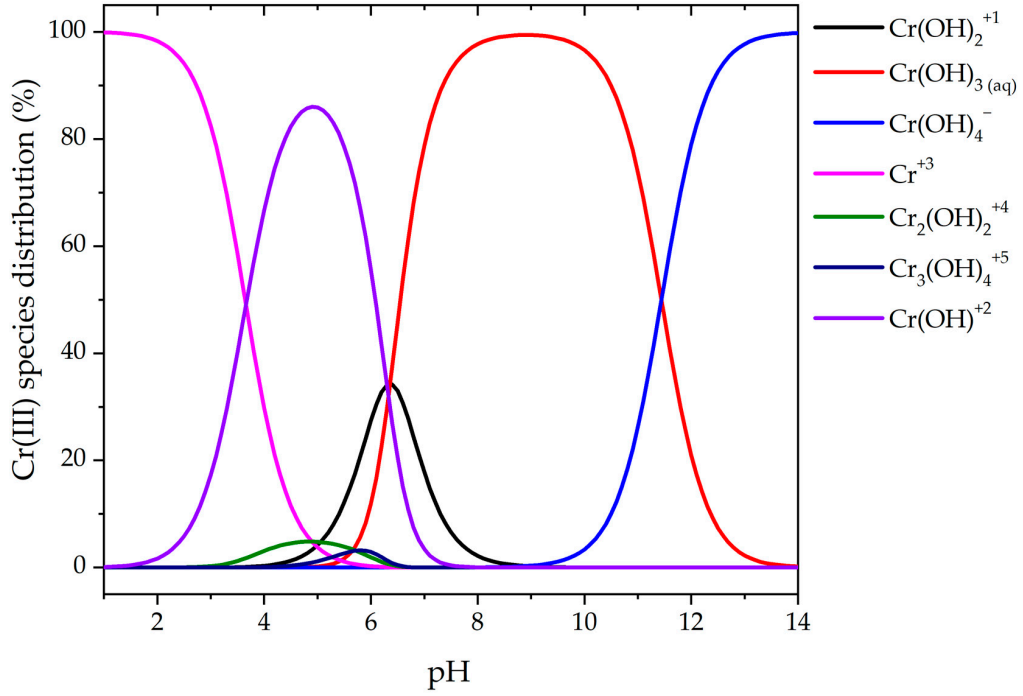


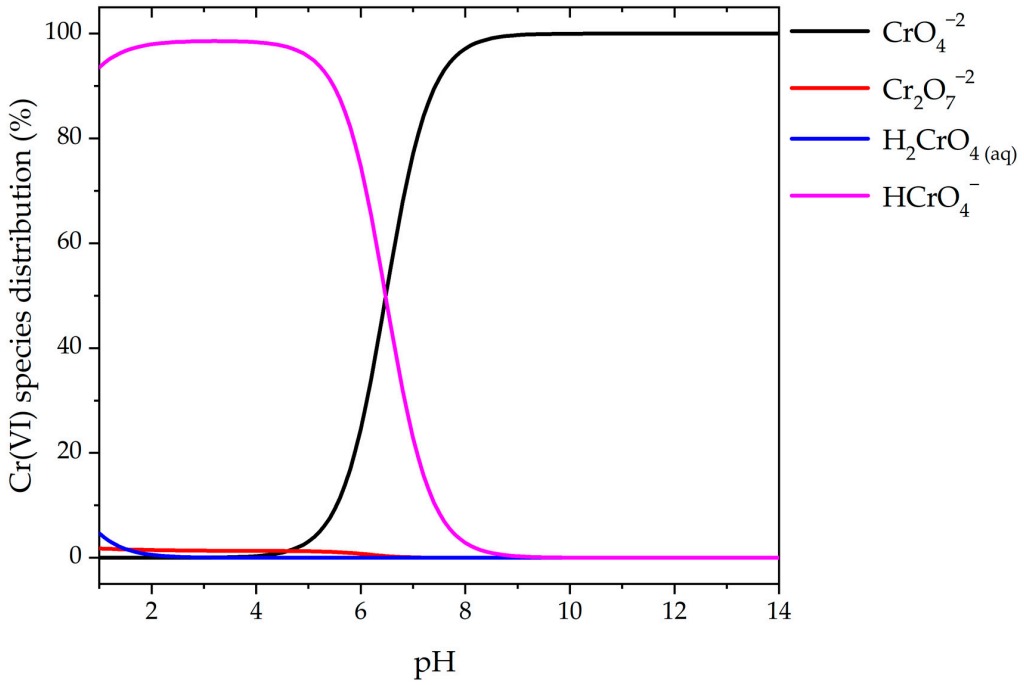
Figure 14. Influence of sequestering agents on the photoreduction of Cr^{6+} and total Cr [5%Ag/Nb_2O_5 (300 °C), additive, pH 2, 1 gL^{-1}, without Air].

Thermodynamic estimates of the speciation of Cr(III) and Cr(VI) ions were performed using the Visual MINTEQ model (Figure 15). The estimations indicated that species percentages of Cr(VI) are dependent on initial concentration and pH value [27]. According to the model, at pH between 2 and 5, $HCrO_4^-$ is the dominant species, whereas at pH above 7, CrO_4^{-2} is more abundant, consistent with the results reported by [28]. For both species, adsorption was favored at lower pH, under the catalyst point of zero charge (6.7 as described in [16]), when the catalyst surface is positively charged. This result justifies the greater efficiency of adsorption and hexavalent chromium reduction at lower pH levels, notably at pH 2. Furthermore, as highlighted by Cappelletti, the reduction in pH increases the driving force for charge transfer at the catalyst surface due to the pH-dependent redox potentials of the Cr(VI)/Cr(III) species [26]. For Cr(III), however, estimates indicated that the predominant species at pH 2 is Cr^{3+}, which is positively charged and whose adsorption on the positively charged catalyst surface is unfavorable. This result explains why it was not possible to reduce Cr(III) to Cr(0), which prevented the removal of total chromium from the solution (Figure 15). The significant impact of adding silver nitrate to the solution (a scavenger of photogenerated electrons) confirms the substantial contribution of the direct charge transfer between the catalyst and the chromium ions. The impact of adding ammonium oxalate (AO) may indicate that radicals generated by the oxidation of formate may also be contributing to the reduction of Cr(VI), although the individual contributions of electrostatic interaction and possible competitive adsorption of formate to pH influence on kinetics could not be quantitatively evaluated in the present work. Interestingly, the addition of AO also allowed for a slight reduction in the total chromium concentration.



(**a**)

Figure 15. *Cont.*



(**b**)

Figure 15. Estimation of Cr(III) (**a**) and Cr(VI) (**b**) speciation at different pH levels.

4. Conclusions

The results suggest that the synthesized 5%Ag/Nb_2O_5 catalyst can be applied efficiently to Cr^{6+} reduction. Using the Nb_2O_5 catalyst resulted in higher efficiency than TiO_2 under the conditions studied. The addition of Ag (promoter) to the catalyst favored the reaction rate. It was observed that calcination at 300 °C, 500 °C, and 700 °C did not significantly affect the results after 120 min of irradiation but did considerably affect the initial kinetics of the process. Some parameters had a more direct impact on the process: pH, additive, air, and catalyst concentration. Another important observation was that adding sodium formate to the catalyst caused it to lose its ability to adsorb chromium on its surface. The best condition found was the use of the Ag-promoted catalyst, 5%Ag/Nb_2O_5 (300 °C), combined with an additive at pH 2, in the absence of O_2 (i.e., in the absence of air). The presence of scavengers (oxalate, silver nitrate, benzoquinone, and isopropanol) influenced the reaction mechanism.

Author Contributions: Methodology, A.K.G.d.S., T.M.P., F.H.S.S.P., M.M.M. and A.L.W.A.; Conceptualization, M.E.K.F. and G.G.L.; Formal Analysis, A.M.T.; Investigation, D.T.D.; Writing—Review and Editing, G.G.L., D.T.D., M.E.K.F., A.M.T., O.A.A.d.S. and E.A. All authors have read and agreed to the published version of the manuscript.

Funding: This research was funded by CNPq, CAPES, Fundação Araucária, C2MMa, and the Programa Ibero-Americano de Ciencia y Tecnología para el Desarrollo (CYTED), through the CATPROH2 network.

Data Availability Statement: The data used to support the findings of this study are included within the article.

Acknowledgments: The authors gratefully acknowledge CNPq, CAPES, Fundação Araucária, C2MMa, and the Programa Ibero-Americano de Ciencia y Tecnología para el Desarrollo (CYTED), through the CATPROH2 network, for their financial support. The authors also acknowledge the Brazilian Mining and Metallurgy Company (CBMM) for their donation of the niobium-containing material used in this research.

Conflicts of Interest: The authors declare no conflicts of interest.

References

1. Zhao, Z.; An, H.; Lin, J.; Feng, M.; Murugadoss, V.; Ding, T.; Liu, H.; Shao, Q.; Mai, X.; Wang, N.; et al. Progress on the Photocatalytic Reduction Removal of Chromium Contamination. *Chem. Rec.* **2019**, *19*, 873–882. [CrossRef] [PubMed]
2. Stambulska, U.Y.; Bayliak, M.M.; Lushchak, V.I. Chromium(VI) Toxicity in Legume Plants: Modulation Effects of Rhizobial Symbiosis. *BioMed Res. Int.* **2018**, *2018*, 8031213. [CrossRef] [PubMed]
3. Nakkeeran, E.; Patra, C.; Shahnaz, T.; Rangabhashiyam, S.; Selvaraju, N. Continuous Biosorption Assessment for the Removal of Hexavalent Chromium from Aqueous Solutions Using Strychnos Nux Vomica Fruit Shell. *Bioresour. Technol. Rep.* **2018**, *3*, 256–260. [CrossRef]
4. Wen, J.; Jiang, T.; Gao, H.; Zhou, W.; Xu, Y.; Zheng, X.; Liu, Y.; Xue, X. An Efficient Utilization of Chromium–Containing Vanadium Tailings: Extraction of Chromium by Soda Roasting–Water Leaching and Preparation of Chromium Oxide. *J. Environ. Manag.* **2019**, *244*, 119–126. [CrossRef] [PubMed]
5. Peng, H.; Guo, J. Removal of Chromium from Wastewater by Membrane Filtration, Chemical Precipitation, Ion Exchange, Adsorption Electrocoagulation, Electrochemical Reduction, Electrodialysis, Electrodeionization, Photocatalysis and Nanotechnology: A Review. *Environ. Chem. Lett.* **2020**, *18*, 2055–2068. [CrossRef]
6. Josué, T.G.; Almeida, L.N.B.; Lopes, M.F.; Santos, O.A.A.; Lenzi, G.G. Cr(VI) Reduction by Photocatalyic Process: Nb_2O_5 an Alternative Catalyst. *J. Environ. Manag.* **2020**, *268*, 110711. [CrossRef] [PubMed]
7. Asoubar, S.; Mehrizad, A.; Behnajady, M.A.; Ramazani, M.E.; Gharbani, P. Hexavalent Chromium Reduction and Rhodamine B Degradation by Visible-Light-Driven Photocatalyst of Stannum Indium Sulfide-Samarium Vanadate. *npj Clean Water* **2023**, *6*, 27. [CrossRef]
8. Yu, M.; Shang, J.; Kuang, Y. Efficient Photocatalytic Reduction of Chromium(VI) Using Photoreduced Graphene Oxide as Photocatalyst under Visible Light Irradiation. *J. Mater. Sci. Technol.* **2021**, *91*, 17–27. [CrossRef]
9. Fidelis, M.Z.; Faria, J.; Santacruz, W.; Lima, T.S.; Lenzi, G.G.; Motheo, A.J. Niobium-Based Catalysts in Advanced Oxidation Processes: A Systematic Review of Mechanisms, Material Engineering, and Environmental Applications. *Environments* **2025**, *12*, 311. [CrossRef]
10. Guillén, C. Band Gap Energy and Lattice Distortion in Anatase TiO_2 Thin Films Prepared by Reactive Sputtering with Different Thicknesses. *Materials* **2025**, *18*, 2346. [CrossRef] [PubMed]
11. Nguyen, V.N.H.; Amal, R.; Beydoun, D. Effect of Formate and Methanol on Photoreduction/Removal of Toxic Cadmium Ions Using TiO_2 Semiconductor as Photocatalyst. *Chem. Eng. Sci.* **2003**, *58*, 4429–4439. [CrossRef]
12. Guo, Y.; Li, L.; Li, Y.; Li, Z.; Wang, X.; Wang, G. Adsorption and Photocatalytic Reduction Activity of Uranium(VI) on Zinc Oxide/Rectorite Composite Enhanced with Methanol as Sacrificial Organics. *J. Radioanal. Nucl. Chem.* **2016**, *310*, 883–890. [CrossRef]
13. Le, Z.; Xiong, C.; Gong, J.; Wu, X.; Pan, T.; Chen, Z.; Xie, Z. Self-Cleaning Isotype g-C_3N_4 Heterojunction for Efficient Photocatalytic Reduction of Hexavalent Uranium under Visible Light. *Environ. Pollut.* **2020**, *260*, 114070. [CrossRef] [PubMed]
14. Li, Y.; Cheng, H.; Jiang, W.; Xie, J.; Xie, Y.; Gao, J.; Ding, Y. Efficient Photocatalytic CO_2 Reduction over Copper-Containing Polyoxometalate Grafted on Blue TiO_2 Catalyst. *Chem. Eng. J.* **2026**, *541*, 177930. [CrossRef]
15. Choi, Y.; Koo, M.S.; Bokare, A.D.; Kim, D.; Bahnemann, D.W.; Choi, W. Sequential Process Combination of Photocatalytic Oxidation and Dark Reduction for the Removal of Organic Pollutants and Cr(VI) Using Ag/TiO_2. *Environ. Sci. Technol.* **2017**, *51*, 3973–3981. [CrossRef] [PubMed]
16. Lenzi, G.G.; Abreu, E.; Fuziki, M.E.K.; Fidelis, M.Z.; Brackmann, R.; de Tuesta, J.L.D.; Gomes, H.T.; dos Santos, O.A.A. 17 α-Ethinylestradiol Degradation in Continuous Process by Photocatalysis Using Ag/Nb_2O_5 Immobilized in Biopolymer as Catalyst. *Top. Catal.* **2022**, *65*, 1225–1234. [CrossRef]
17. Liu, X.X.; Qin, C.; Cao, L.; Feng, Y.; Huang, Y.; Qin, L.; Seo, H.J. A Silver Niobate Photocatalyst $AgNb_7O_{18}$ with Perovskite-like Structure. *J. Alloys Compd.* **2017**, *724*, 381–388. [CrossRef]
18. Liu, X.; Qin, C.; Huang, Y.; Qin, L.; Seo, H.J. A New Silver Niobate Photocatalyst $AgNb_{13}O_{33}$: Synthesis, Structure and Photochemical Properties. *J. Taiwan Inst. Chem. Eng.* **2017**, *78*, 530–538. [CrossRef]
19. Rozier, P.; Szajwaj, O. Crystal Chemistry in the Ag_2O-Nb_2O_5 System. $AgNb_3O_8$ Structure Determination. *J. Solid State Chem.* **2008**, *181*, 228–234. [CrossRef]
20. Liu, Y.; Shao, L.; Zhang, S.; Hu, L.; Wu, Y.; Liu, C.; Huang, Y.; Le, P.; Li, W.; Xue, N.; et al. Effect of Chemical Composition and Heat Treatment on the Microstructure and Performance of Ag-Based Alloy Wires. *Mater. Des.* **2025**, *258*, 114728. [CrossRef]
21. Dias, D.T.; Rodrigues, A.O.; Pires, P.B.; Semianko, B.C.; Fuziki, M.E.K.; Lenzi, G.G.; Sabino, S.R.F. Photoacoustic Spectroscopy of Titanium Dioxide, Niobium Pentoxide, Titanium:Niobium, and Ruthenium-Modified Oxides Synthesized Using Sol-Gel Methodology. *Appl. Spectrosc.* **2024**, *78*, 1028–1042. [CrossRef] [PubMed]

22. Pires, P.B.; Fuziki, M.E.K.; Lenzi, G.G.; Sabino, S.d.R.F.; Novatski, A.; Tebcherani, S.M.; Dias, D.T. Effect of Pressure-Assisted Heat Treatment on the Crystalline Phase of Titanium Dioxide, Niobium Pentoxide, and Ruthenium-Modified Oxides. *ACS Omega* **2026**, *11*, 7680–7690. [CrossRef] [PubMed]
23. Lenzi, G.G.; Lopes, M.F.; Andrade, D.I.; Napoli, J.S.; Parolin, A.; Fávaro, Y.B.; Kounaris Fuziki, M.E.; de Almeida, L.N.B.; Josué, T.G.; Dias, D.T.; et al. Functioned Catalysts with Magnetic Core Applied in Ibuprofen Degradation. *Water Sci. Technol.* **2021**, *84*, 2158–2179. [CrossRef] [PubMed]
24. Das, A.J.; Kumar, R.; Goutam, S.P. Sunlight Irradiation Induced Synthesis of Silver Nanoparticles Using Glycolipid Bio-Surfactant and Exploring the Antibacterial Activity. *J. Bioeng. Biomed. Sci.* **2016**, *6*, 208–213. [CrossRef]
25. Samson, O.; Adeeko, T.O.; Makama, E.K. Synthesis and Optical Characterization of Silver Nanoparticles (Ag-NPs) Thin Films (TFs) Prepared by Silar Technique. *Int. J. Curr. Res. Acad. Rev.* **2017**, *5*, 15–24. [CrossRef]
26. Cappelletti, G.; Bianchi, C.L.; Ardizzone, S. Nano-Titania Assisted Photoreduction of Cr(VI). *Appl. Catal. B* **2008**, *78*, 193–201. [CrossRef]
27. Gao, X.; Guo, C.; Hao, J.; Zhang, Y.; Li, M.; Zhao, Z. Efficient Removal of Cr(VI) by Modified Sodium Alginate via Synergistic Adsorption and Photocatalytic Reduction. *Appl. Surf. Sci.* **2022**, *579*, 152259. [CrossRef]
28. Thakur, R.S.; Chaudhary, R.; Singh, C. Influence of PH on Photocatalytic Reduction, Adsorption, and Deposition of Metal Ions: Speciation Modeling. *Desalin. Water Treat.* **2015**, *56*, 1335–1363. [CrossRef]

Disclaimer/Publisher's Note: The statements, opinions and data contained in all publications are solely those of the individual author(s) and contributor(s) and not of MDPI and/or the editor(s). MDPI and/or the editor(s) disclaim responsibility for any injury to people or property resulting from any ideas, methods, instructions or products referred to in the content.